# The Chd4 Helicase Regulates Chromatin Accessibility and Gene Expression Critical for β-Cell Function In Vivo

Rebecca K. Davidson,[1,2,3] Sukrati Kanojia,[1,2,3] Wenting Wu,[2,4] Tatsuyoshi Kono,[1,2,3] Jerry Xu,[2,3,5] Meredith Osmulski,[2,3,5] Robert N. Bone,[2,3] Nolan Casey,[2,3] Carmella Evans-Molina,[1,2,3,5,6,7,8] Emily K. Sims,[1,2,3,5] and Jason M. Spaeth[1,2,3,5,7]

*Diabetes 2023;72:746–757 | https://doi.org/10.2337/db22-0939*

**The transcriptional activity of Pdx1 is modulated by a diverse array of coregulatory factors that govern chromatin accessibility, histone modifications, and nucleosome distribution. We previously identified the Chd4 subunit of the nucleosome remodeling and deacetylase complex as a Pdx1-interacting factor. To identify how loss of Chd4 impacts glucose homeostasis and gene expression programs in β-cells in vivo, we generated an inducible β-cell–specific Chd4 knockout mouse model. Removal of *Chd4* from mature islet β-cells rendered mutant animals glucose intolerant, in part due to defects in insulin secretion. We observed an increased ratio of immature-to-mature insulin granules in *Chd4*-deficient β-cells that correlated with elevated levels of proinsulin both within isolated islets and from plasma following glucose stimulation in vivo. RNA sequencing and assay for transposase-accessible chromatin with sequencing showed that lineage-labeled *Chd4*-deficient β-cells have alterations in chromatin accessibility and altered expression of genes critical for β-cell function, including *MafA*, *Slc2a2*, *Chga*, and *Chgb*. Knockdown of *CHD4* from a human β-cell line revealed similar defects in insulin secretion and alterations in several β-cell–enriched gene targets. These results illustrate how critical Chd4 activities are in controlling genes essential for maintaining β-cell function.**

### ARTICLE HIGHLIGHTS

- Pdx1–Chd4 interactions were previously shown to be compromised in β-cells from human donors with type 2 diabetes.
- β-Cell–specific removal of Chd4 impairs insulin secretion and leads to glucose intolerance in mice.
- Expression of key β-cell functional genes and chromatin accessibility are compromised in Chd4-deficient β-cells.
- Chromatin remodeling activities enacted by Chd4 are essential for β-cell function under normal physiological conditions.

Chromatin is a dynamic molecular structure of DNA and nucleosomes, which are histone octamers that serve to package the eukaryotic genome and regulate accessibility of DNA for recombination, damage repair, replication, and transcription. Since the occupancy of nucleosomes along the DNA strand hinders access of transcriptional regulators, modulation of chromatin accessibility is a major control point in gene expression. Movement of nucleosomes along the DNA strand is facilitated by multiprotein chromatin-remodeling complexes that use the energy derived from ATP hydrolysis to exchange, slide, or evict histones (1). Maintenance of transcriptional regulation by these complexes is largely mediated by recruitment to

[1]Department of Biochemistry and Molecular Biology, Indiana University School of Medicine, Indianapolis, IN
[2]Center for Diabetes and Metabolic Diseases, Indiana University School of Medicine, Indianapolis, IN
[3]Herman B Wells Center for Pediatric Research, Indiana University School of Medicine, Indianapolis, IN
[4]Department of Medical and Molecular Genetics, Indiana University School of Medicine, Indianapolis, IN
[5]Department of Pediatrics, Indiana University School of Medicine, Indianapolis, IN
[6]Department of Medicine, Indiana University School of Medicine, Indianapolis, IN
[7]Department of Anatomy, Cell Biology, and Physiology, Indiana University School of Medicine, Indianapolis, IN
[8]Richard L. Roudebush Veterans' Administration Medical Center, Indianapolis, IN
Corresponding author: Jason M. Spaeth, jspaeth@iu.edu

Received 9 November 2022 and accepted 1 March 2023
This article contains supplementary material online at https://doi.org/10.2337/figshare.22236679.

specific promoter or enhancer genomic loci regions in a transcription factor (TF)-dependent manner.

Transcriptional dysregulation is the basis of numerous diseases, including type 2 diabetes (T2D). It was demonstrated that a subset of failing human islet β-cells from donors with T2D lose activity and expression of islet-enriched TFs, including PDX1, NKX6.1, and MAFA (2). Under physiological conditions, these TFs direct the transcription of genes essential for glucose-stimulated insulin secretion (GSIS), including *Ins*, components of glucose transport and metabolism (e.g., *Slc2a2*, *Gck*), components of $K_{ATP}$ channels and voltage-gated calcium pumps (e.g., *Kcnj11*, *Abcc8*, *Vdccβ*, *Vdccα1D*, *Serca2b*, *Serca3*), and components necessary for hormone processing and insulin granule exocytosis (e.g., *Pcsk1*, *Pcsk2*, *Cpe*, *Stx1a*, *Stxbp1*, *Snap25*, *Vamp2*, *Vamp3*, *Syt4*, *Sytl4*) (3). Loss of transcriptional activity of key islet-enriched TFs leads to reduced expression of these components necessary for GSIS, impaired β-cell function, and ultimately overt diabetes. Therefore, it is of critical importance to understand the mechanisms by which TFs control expression of genes to maintain GSIS under physiological conditions and how their activities become disrupted in settings of T2D.

Numerous transcriptional coregulators have been identified to modulate the activity of β-cell–specific TFs and to play a role in maintaining β-cell function in vivo. For example, conditional whole-islet deletion of Ldb1 impaired Isl-1 target gene expression in α- and β-cells and led to hyperglycemia and reduced hormone production (4,5). Additionally, conditional deletion of the Mll3/4 subunit NCoA6 in mouse β-cells impaired transcription of MafA target genes and ex vivo GSIS (6). Similarly, β-cell–specific deletion of Swi/Snf chromatin remodeling activity in mice impaired binding of Pdx1 to Ins2, which blunted insulin production leading to impaired whole-body glucose homeostasis (7).

Recently, our group demonstrated that the chromodomain helicase 4 (Chd4) subunit of the nucleosome remodeling and deacetylase (NuRD) complex is required to maintain β-cell function in vitro (8). We found that Chd4 dynamically interacts with the essential β-cell TF, Pdx1, in mouse and human β-cell lines and primary tissue. In vivo, acute glucose stimulation enhanced Pdx1–Chd4 interactions, and transient reduction of *Chd4* in rodent β-cell lines impaired GSIS. Interestingly, interactions between Pdx1 and Chd4 are severely impacted in T2D settings, as β-cells from tissue of mice fed a high-fat diet and tissue of human donors with T2D contained significantly fewer interactions compared with tissue of mice fed a normal diet or tissue of donors without diabetes, respectively.

Based on these findings and the profound observation that loss of CHD4-PDX1 complex formation is a significant feature of T2D pathophysiology (8), further evaluation is necessary to uncover the mechanistic basis by which Chd4 modulates the chromatin landscape and gene expression programs required for optimal β-cell function in vivo. To this end, we generated a tamoxifen-inducible β-cell–specific *Chd4*-deficient mouse model. We demonstrate that loss of Chd4 from the mature β-cell impairs whole-body glucose homeostasis and islet insulin secretion and leads to increased immature insulin granules and excess proinsulin throughout *Chd4*-deficient β-cells. These alterations were found to be the consequence of a disordered chromatin landscape and differential gene expression programs critical for normal β-cell function, several of which were confirmed following *CHD4* knockdown in human β-cell lines. Collectively, our results highlight a predominant role for Chd4 in controlling gene expression signatures in adult β-cells.

## RESEARCH DESIGN AND METHODS

### Animal Models

*MIP-Cre$^{ERT}$* (9) mice were used to remove the *LoxP* sites flanking exons 12 and 21 of the *Chd4* locus (*Chd4$^{f/f}$* [10]) and the stop cassette in the *Rosa26-Loxp-Stop-Loxp-tdTomato* lineage reporter (*R26$^{LSL\text{-}tdTomato}$* [11]). The following genotypes were used: control (*MIP-Cre$^{ERT}$;Chd4$^{f/+}$;R26$^{LSL\text{-}tdTomato/+}$*) and *Chd4$^{\Delta\beta}$* (*MIP-Cre$^{ERT}$;Chd4$^{f/f}$;R26$^{LSL\text{-}tdTomato/+}$*). Cre$^{ERT}$-mediated recombination of *Chd4$^{f/f}$* and the *R26$^{LS\text{-}LtdTomato}$* was achieved through administration of 100 mg/kg tamoxifen (T5648; Sigma-Aldrich) by oral gavage once per day for a 5-day period.

### Intraperitoneal Glucose Tolerance Test and Plasma Insulin/Proinsulin Measurements

Mice ($n$ = 10–18) were given an injection of D-glucose in PBS (2 mg/g body wt i.p.) after a 6-h fast. Blood glucose was measured with an AimStrip Plus Blood Glucose Meter (Germaine Laboratories). Plasma insulin under ad libitum feeding conditions or following a 6-h fast was collected and measured by radio immunoassay at the Translation Core at Indiana University School of Medicine. For glucose-stimulated plasma insulin and proinsulin measurements, plasma was collected 2 min following injection with D-glucose (2 mg/g body wt) and measured by radio immunoassay or ELISA.

### Tissue Preparation and Microscopy

Whole mouse pancreata were isolated and fixed for 4 h in 4% (v/v) paraformaldehyde and then washed three times in PBS and placed in 30% sucrose overnight at 4°C. The following day, pancreata were embedded in optimal cutting temperature embedding medium and frozen in a −80°C freezer. Sections were generated at 6-μm thickness on a cryostat (Leica Biosystems). We performed immunofluorescence staining by incubating slides with primary antibodies, described in Supplementary Table 1.

Images were acquired on a Zeiss LSM 800 confocal laser scanning microscope and processed with ImageJ software. For β-cell area quantitation, six sections (∼300 μm apart) from control and *Chd4$^{\Delta\beta}$* mice were analyzed for insulin staining with use of 3,3′-diaminobenzidine substrate and counterstained with eosin. The percentage of insulin$^{+}$ area relative to pancreas area was calculated. For quantitation of immunofluorescence images, we restricted the quantitation to the Tomato$^{+}$ area using a mask function in Image J and

subsequently measuring the pixel intensities of MafA, CgA, and CgB staining.

### Perifusion of Isolated Islets

Islets were isolated (12) and perifusion was performed by the Islet and Physiology Core at Indiana University School of Medicine. Insulin secretion samples were measured with ELISA by the Translation Core at Indiana University School of Medicine. Insulin secretion was normalized to DNA content as measured with the Quant-iT PicoGreen dsDNA Assay Kits and dsDNA Reagents (P7589; Invitrogen).

### Cytoplasmic $Ca^{2+}$ Imaging

For measurement of intracellular $Ca^{2+}$, isolated islets were incubated in 5.5 mmol/L glucose media for 48 h and loaded with the ratiometric $Ca^{2+}$ indicator Fura-2 acetoxymethyl ester (Fura-2, AM) (8 μmol/L, F-1221; Invitrogen) and 0.04% Pluronic F127. Islets were transferred for imaging to a glass-bottom plate containing Hanks' balanced salt solution supplemented with 0.2% BSA, 1.0 mmol/L $Mg^{2+}$, 2.0 mmol/L $Ca^{2+}$, and 5.5 mmol/L glucose for baseline measurements. Plates were mounted on the stage of a Zeiss Axio Observer microscope and incubated at 37°C with use of an in-line heater (Pecon) for 10–15 min before being perifused with either 16.7 mmol/L glucose or 30 mmol/L KCl. Excitation light from a xenon burner was supplied to the preparation via a light pipe and filter wheel (Sutter Instrument Company). Images were taken sequentially under conditions of 340 nm and then 380 nm excitation with a Hamamatsu ORCA-ER camera for production of data representing each intracellular $Ca^{2+}$ ratio from emitted light at 510 nm.

### Transmission Electron Microscopy and Granule Quantitation

Approximately 1,000 isolated islets from four control and five *Chd4*$^{\Delta\beta}$ animals were suspended separately in 100 μL media and 100 μL 2% glutaraldehyde + 4% paraformaldehyde in 0.1 mol/L sodium cacodylate for 10 min. Supernatant was removed and 500 μL fixative was added to the islets for 1 h. Fixative was removed and replaced with fresh fixative, and islets were resuspended. The fixed islets were sent to the Advanced Electron Microscopy Core Facility at the University of Chicago for further processing and imaging.

Mature and immature insulin granules were quantitated with the ImageJ Cell Counter plugin. Granules were quantitated as a percentage of mature, immature, or rod like divided by the total number of counted granules in each image. A total of 20 images were quantitated per group.

### Flow Cytometry and RNA Purification

Isolated islets were dispersed into a single-cell suspension (Accumax, A7089; Sigma-Aldrich), stained with DAPI, and sorted by gating for Tomato$^+$DAPI$^+$ cells with FACS at the Indiana University School of Medicine Flow Cytometry Resource Facility. RNA was isolated from FACS-purified β-cells (mean ± SEM 30,648 ± 6,565 cells [control; $n$ = 4] and 18,725 ± 3,161 cells [*Chd4*$^{\Delta\beta}$; $n$ = 4]) with use of the RNAqueous-Micro kit and analyzed on 2100 Bioanalyzer (Agilent Technologies). Only samples with an RNA integrity number >7.5 were used for cDNA synthesis and library preparation.

### RNA Sequencing and Analysis

One nanogram of total RNA per sample was used for library preparation. cDNA was first synthesized with use of SMART-Seq v4 Ultra Low Input RNA Kit for Sequencing (Takara Bio). A dual indexed cDNA library was then prepared with use of Nextera XT DNA Library Prep Kit (Illumina). Each library was quantified and its quality accessed with Qubit and Agilent Bioanalyzer, and multiple libraries were pooled in equal molarity. The average size of the library insert was ∼300–400 base pairs (bp). The pooled libraries were then denatured and neutralized before loading to the NovaSeq 6000 sequencer for 100b paired-end sequencing (Illumina). Approximately 30–40 × $10^6$ reads per library were generated. A Phred quality score (Q score) was used to measure the quality of sequencing. More than 95% of the sequencing reads reached Q30 (99.9% base call accuracy). The generated FASTQ files were processed with the Genialis visual informatics platform (https://www.genialis.com).

### Assay for Transposase-Accessible Chromatin With Sequencing and Analysis

A total of 27,000–80,000 Tomato$^+$ mature β-cells were collected for assay for transposase-accessible chromatin with sequencing (ATAC-Seq). Cells were first lysed to collect nuclei through incubating with 100 μL lysis buffer (10 mmol/L Tris-HCl, 10 mmol/L NaCl, 3 mmol/L $MgCl_2$, 0.10% Tween-20, 0.10% Nonidet P40 Substitute, 0.01% Digitonin, 1% BSA, 1 mmol/L dithiothreitol [DTT], 40 units/μL RNase Inhibitor) for 3 min, centrifuging at 300 rcf for 5 min at 4°C, and discarding the supernatant. The resulting nuclei were then washed with 1 mL wash buffer (10 mmol/L Tris-HCl, 10 mmol/L NaCl, 3 mmol/L $MgCl_2$, 0.10% Tween-20, 1% BSA, 1 mmol/L DTT, 40 units/μL RNase Inhibitor) and centrifuged at 200 rcf for 5 min at 4°C two to three times. The final nuclei, ranging from 14,000 to 45,000 in number, were used for tagmentation and library preparation following procedures previously described (13). In brief, the nuclei were immediately suspended in 50 μL tagmentation reaction with use of 2× TD Buffer (FC-121-1030; Illumina) and Nextera Tn5 Transposase enzyme (FC-121-1030; Illumina). Fragments >600 bp were excluded in library preparation. Each resulting indexed library was quantified and its quality assessed with Qubit and Agilent Bioanalyzer, and multiple libraries were pooled in equal molarity. The pooled libraries were then denatured and neutralized before loading to NovaSeq 6000 sequencer at 300 pmol/L final concentration for 100b paired-end sequencing (Illumina). Approximately 100 × $10^6$ reads per library were generated. A Phred quality score (Q score)

was used to measure the quality of sequencing. More than 90% of the sequencing reads reached Q30 (99.9% base call accuracy).

### Motif Analysis Using HOMER

HOMER (Hypergeometric Optimization of Motif EnRichment) (14) was used to perform motif enrichment analysis on those differentially accessible chromatins (DAC) and enhancer regions that were found in *Chd4*$^{\Delta\beta}$ β-cells. The search lengths of the motifs were 10 bp. *P* values were calculated through comparison of the enrichments within the target regions with those of a random set of regions (background) generated by HOMER.

### RNA Interference–Mediated Chd4 Knockdown in EndoC-βH1 Cell Line

Human EndoC-βH1 cells (15) were cultured at 37°C in 5% $CO_2$ in low glucose (1 g/L) DMEM, 2% albumin from bovine serum fraction V, 50 μmol/L 2-mercaptoethanol, 10 mmol/L nicotinamide, 5.5 μg/mL transferrin, 6.7 ng/mL sodium selenite, and 1% PSA with passage numbers ranging between 85 and 95. siRNA knockdown in EndoC-βH1 cells was achieved with use of ON-TARGETplus siRNAs targeting human CHD4 (no. L-009774-00; Dharmacon). Targeting siRNA or a nontargeting control (no. D-001810-10; Dharmacon) was diluted in Opti-MEM and incubated with Lipofectamine RNAiMAX (LMRNA015; Invitrogen) at a 1:3 ratio for 5 min. Cells suspended in Opti-MEM were combined with the mixture of siRNA and Lipofectamine RNAiMAX at a density of $2 \times 10^6$ cells in a 6-well dish until adherent, and then media was replaced with EndoC-βH1 growth media. GSIS was performed and RNA and nuclear extracts were collected 72 h after transfection. Nuclear extracts were resolved by SDS-PAGE and immunoblotted with CHD4 and β-actin antibodies. RNA was purified per the manufacturer's instructions (D7001; Zymo Research) and cDNA prepared (4368814; Applied Biosystems). Quantitative PCR reactions were performed with the gene primers listed in Supplementary Table 2 on a QuantStudio 3 Real-Time PCR System (A28567; Applied Biosystems). Gene expression changes were analyzed with the $2^{-\Delta\Delta CT}$ method (16) with use of *GAPDH* for normalization. For GSIS, cells were treated with baseline glucose solution at 1 mmol/L glucose for 1 h. Cells were then treated with either 2.8 mmol/L glucose (low) or 16.7 mmol/L glucose (high) for 1 h. Secretion media were collected, and cells were treated with acid/ethanol solution for collection of contents. Human insulin and proinsulin ELISAs were performed by the Translation Core at Indiana University School of Medicine. Insulin secretion samples were normalized to insulin content.

### Statistical Analysis

Statistical significance was determined with the two-tailed Student *t* test for comparison of two experimental groups or one-way ANOVA with Tukey post hoc analysis for comparing more than two groups. Data are presented as means ± SEM. A threshold of $P < 0.05$ was used to declare significance.

### Study Approval

All animal studies were reviewed and approved by the Indiana University Institutional Animal Care and Use Committee. Mice were housed and cared for according to the Indiana University Laboratory Animal Resource Center and the Institutional Animal Care and Use Committee/Office of Animal Welfare Assurance standards and guidelines.

### Data and Resource Availability

Raw and analyzed RNA-sequencing and ATAC-Seq data sets have been deposited in Gene Expression Omnibus (GEO) (accession no. GSE217446). All noncommercially available resources generated and/or analyzed during the current study are available from the corresponding author on reasonable request.

## RESULTS

### Adult Islet β-Cell Function Is Impaired Following Loss of Chd4

To evaluate the contributions of Chd4 in controlling β-cell function in vivo, we crossed transgenic mice containing a tamoxifen-inducible, β-cell–specific Cre recombinase (mouse *Ins1* enhancer/promoter [*MIP*]-driven *Cre*$^{ERT}$ [9]) and the *Rosa26-Loxp-Stop-Loxp-tdTomato* (*R26*$^{LSL\text{-}tdTomato}$ [11]) lineage reporter with mice containing LoxP sites flanking exons 12–21 of the *Chd4* gene (i.e., *Chd4*$^{\Delta\beta}$ [10]) (Supplementary Fig. 1*A* and *B*). All experimental and control (*MIP-Cre*$^{ERT}$;*Chd4*$^{f/+}$) animals contain the *MIP-Cre*$^{ERT}$ transgene and received tamoxifen, as this line has been shown to augment islet β-cell mass and function independently (17,18). Removal of *Chd4* was achieved through administration of five doses of tamoxifen over a 5-day period. Four weeks following the last tamoxifen dose, immunofluorescence analysis confirmed removal of Chd4 protein from the majority of β-cells throughout the islets of *Chd4*$^{\Delta\beta}$ mice (Supplementary Fig. 1*C* and *D*).

Male *Chd4*$^{\Delta\beta}$ mutants displayed impaired glucose tolerance 4 weeks following the last tamoxifen treatment with no alterations in body weight (Fig. 1*A* and Supplementary Fig. 2*A*). Importantly, we compared *MIP-Cre*$^{ERT}$–positive mice (*MIP-Cre*$^{ERT}$;*Chd4*$^{+/+}$) with our controls (*MIP-Cre*$^{ERT}$;*Chd4*$^{f/+}$), which revealed no change in glucose tolerance between the Cre-alone animals and heterozygous controls (Supplementary Fig. 2*B*). Based on the breeding strategies, efforts to use control and experimental littermates, and the similar phenotypes between *MIP-Cre*$^{ERT}$–positive and *MIP-Cre*$^{ERT}$;*Chd4*$^{f/+}$ mice, we selected the latter as the control cohort throughout. Female *Chd4*$^{\Delta\beta}$ mutants also displayed the glucose intolerance phenotype at 4 weeks post–tamoxifen treatment, although not as severe as male littermates (Supplementary Fig. 2*C*). Moreover, the phenotype did not appear to become worse as the animals age, as at 8 weeks post–tamoxifen treatment glucose tolerance in female *Chd4*$^{\Delta\beta}$ mutants was similar to that at 4 weeks (Fig. 1*A* and

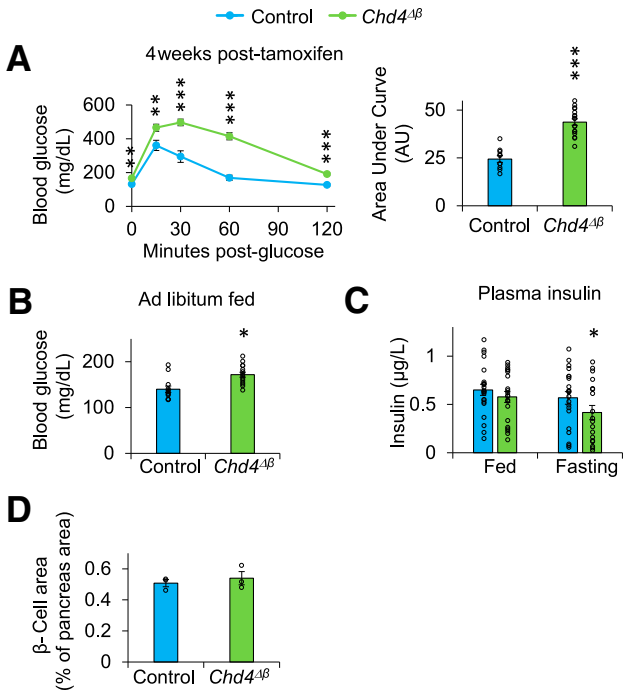


**Figure 1**—Glucose tolerance is impaired and insulin levels are reduced in male *Chd4*$^{\Delta\beta}$ mice. *A*: Glucose tolerance was compromised in *Chd4*$^{\Delta\beta}$ male mice during intraperitoneal glucose tolerance tests 4 weeks following the last tamoxifen treatment. Area under the curve analysis of glucose tolerance tests is shown graphically ($n$ = 10–17). AU, arbitrary units. *B*: Ad libitum feeding blood glucose levels were elevated in *Chd4*$^{\Delta\beta}$ male mice ($n$ = 10–17). *C*: Plasma insulin levels were reduced in fasted *Chd4*$^{\Delta\beta}$ male animals ($n$ = 15–18). *$P$ < 0.05; **$P$ < 0.01; ***$P$ < 0.001. *D*: β-Cell area is unchanged between control and *Chd4*$^{\Delta\beta}$ male animals ($n$ = 3).

Supplementary Fig. 2*C* and *D*). Ad libitum feeding blood glucose levels were elevated in male and female *Chd4*$^{\Delta\beta}$ mutants, and plasma insulin levels were reduced in male, but not female, mutants (Fig. 1*B* and *C* and Supplementary Fig. 2*E* and *F*). The defect in glucose homeostasis and reduced plasma insulin levels suggested that there could be a decrease in islet β-cell area; however, analyses from 4 weeks post–tamoxifen treatment in male mutants show no difference (Fig. 1*D*).

As β-cell area was unchanged, we queried whether insulin secretion from male *Chd4*$^{\Delta\beta}$ mutant islets was impaired. Islet perifusion analysis was used to examine the dynamics of insulin secretion ex vivo at rest (2.5 mmol/L glucose), in response to 16.7 mmol/L glucose, and in response to 2.5 mmol/L glucose with direct depolarization by 30 mmol/L KCl. As expected, based on in vitro Chd4 knockdown followed by GSIS in rat INS-1 832/13 β-cell lines (8), *Chd4*$^{\Delta\beta}$ mutant islets have a marked reduction in insulin secretion at steady state, 1st phase, and 2nd phase and under KCl-induced depolarizing conditions (Fig. 2*A* and *B*).

The profound defects in insulin release following glucose stimulation and KCl-induced depolarization suggested that stimulation of $Ca^{2+}$ influx through voltage-sensitive $Ca^{2+}$ channels could be altered. Therefore, $Ca^{2+}$ imaging experiments using the ratiometric $Ca^{2+}$ indicator Fura-2, AM, were conducted in islets from male control and *Chd4*$^{\Delta\beta}$ mutants. Remarkably, while phase 1 duration was modestly expedited in *Chd4*$^{\Delta\beta}$ islets, no alterations were observed in baseline $Ca^{2+}$ flux prior to glucose stimulation or phase 1 amplitude, oscillatory amplitude, or oscillatory duration after glucose stimulation (Supplementary Fig. 3). Moreover, islets treated with 2.5 mmol/L glucose and 30 mmol/L KCl presented with no change in cytosolic $Ca^{2+}$ (Fig. 2*C*). Collectively, these observations indicate that the insulin secretion defects are largely independent of $Ca^{2+}$ flux dynamics.

### Expression of Key β-Cell Functional Genes Is Compromised in *Chd4*$^{\Delta\beta}$ β-Cells

To define the molecular influence of Chd4 in controlling gene expression programs within the β-cell, we performed

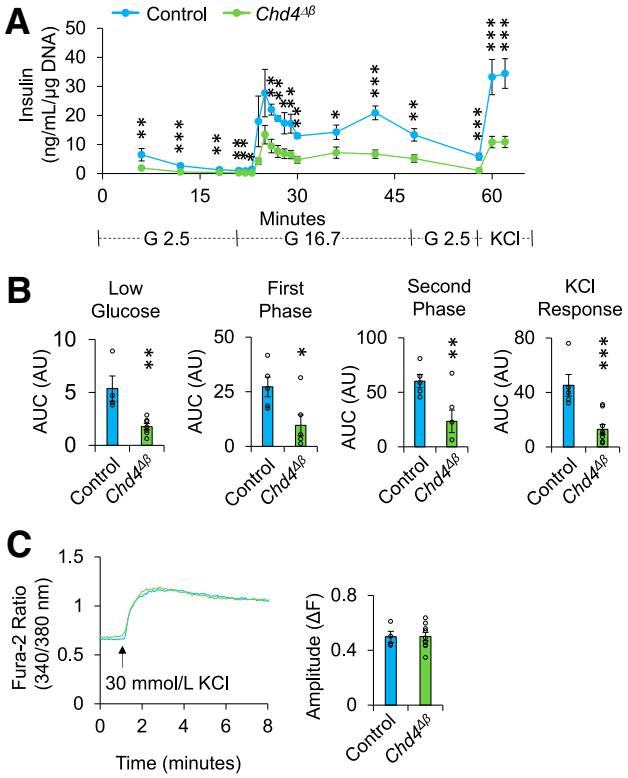


**Figure 2**—Glucose and KCl-stimulated insulin release of perifused islets is impaired in *Chd4*$^{\Delta\beta}$ islets. *A* and *B*: Insulin secretion from perifused control and *Chd4*$^{\Delta\beta}$ male islets at 2.5 mmol/L glucose (G), 16.7 mmol/L glucose, and 2.5 mmol/L glucose + 30 mmol/L KCl. *B*: Corresponding area under the curve (AUC) analysis of insulin secretion during low glucose (2.5 mmol/L glucose), 16.7 mmol/L glucose–stimulated first phase (21–30 min) and second phase (30–48 min), and 2.5 mmol/L glucose + 30 mmol/L KCl stimulation (48–62 min) ($n$ = 4–5). AU, arbitrary units. *C*: Representative trace of intracellular $Ca^{2+}$ measurements from isolated male islets with use of ratiometric $Ca^{2+}$ indicator Fura-2, AM, under stimulation with 30 mmol/L KCl. The amplitude (ΔF) of intracellular $Ca^{2+}$ is unchanged in *Chd4*$^{\Delta\beta}$ islets, indicating that KCl-mediated defect in insulin secretion is not due to $Ca^{2+}$ ($n$ = 4–8). *$P$ < 0.05; **$P$ < 0.01; ***$P$ < 0.001.

RNA sequencing on FACS Tomato$^{+}$ β-cells from dispersed male control and *Chd4*$^{\Delta\beta}$ islets. Using a twofold cutoff and false discovery rate of <0.05, we found 438 down- and 1,093 upregulated genes in *Chd4*$^{\Delta\beta}$ β-cells (Fig. 3*A* and Supplementary Table 3). Several of the genes with reduced expression include those encoding the MafA TF (*MafA*), islet secretory granule molecules chromogranin A (*Chga*) and chromogranin B (*Chgb*), the $Ca^{2+}$-binding synaptotagmin 10 (*Syt10*), the primary glucose transporter Glut2 (*Slc2a2*), and roundabout receptor 2 (*Robo2*) and its ligand *Slit1*—all critical factors in β-cell physiology (19). We confirmed the reduction of several of these important modulators of insulin production and secretion at the protein level, including MafA, CgA, and CgB (Fig. 4). Additionally, disallowed genes *Hk2*, *Pdgfra2*, and *Mycl*, and numerous *Serpina* and *Serpine* genes, were upregulated in *Chd4*$^{\Delta\beta}$ β-cells (Fig. 3*A* and *B* and Supplementary Table 3). The Serpina family of genes cluster together on chromosome 12 and are downregulated in the late stages of the secondary transition, a temporary point critical for endocrine cell development (20). *SERPINE2* expression has been shown to be upregulated in T2D donor islets (21), further highlighting that the transcriptional programming governed by Chd4 is closely linked to diabetes pathogenesis. Moreover, we observed no significant alterations in expression of fundamental islet-enriched TF mRNAs (e.g., *Foxo1*, *Hnf1b*, *Isl1*, *Mnx1*, *Neurod1*, *Nkx2.2*, *Pax6*, *Pdx1*) (Supplementary Fig. 4*A* and *B*). Lastly, we found no increased levels of glucagon or somatostatin in Tomato$^{+}$ *Chd4*$^{\Delta\beta}$ β-cells (Supplementary Fig. 4*B*), supporting that loss of Chd4 does not lead to aberrant expression of α-cell– and δ-cell–enriched genes.

As Chd4 has been shown to interact with Pdx1 and play instrumental roles in maintaining Pdx1 function (8), we compared those genes differentially expressed in *Chd4*$^{\Delta\beta}$ β-cells with genes bound by Pdx1 in mouse islets (22), which revealed a partial overlap of 385 genes. Gene ontology (GO) analysis of these genes with use of the Database for Annotation, Visualization, and Integrated Discovery (DAVID) led to the identification of pathways linked to hormone secretion and regulation of $K^{+}$ ion transmembrane transport (Fig. 3*C*), the latter of which is supported by the significant defect in insulin secretion when *Chd4*$^{\Delta\beta}$

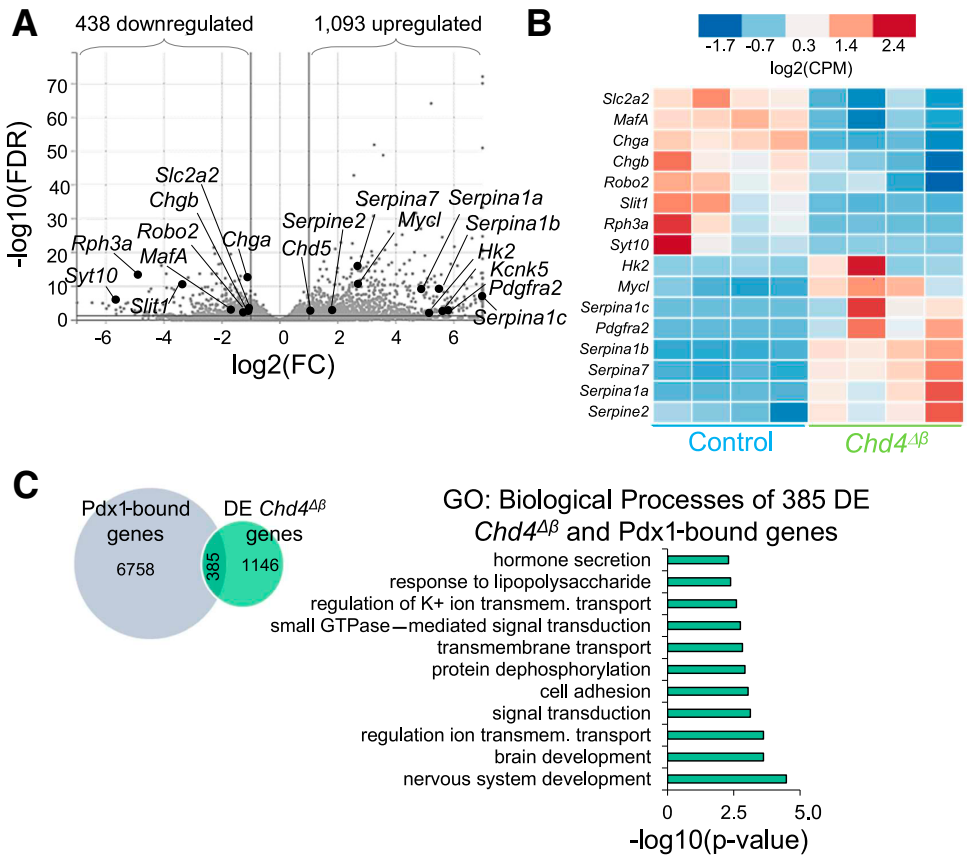


**Figure 3**—RNA sequencing identifies Pdx1-bound genes differentially expressed in *Chd4*$^{\Delta\beta}$ β-cells. *A*: Volcano plot illustrating the most DEGs in FACS-sorted, Tomato$^{+}$ *Chd4*$^{\Delta\beta}$ male β-cells. *B*: Heat map hierarchical clustering displaying log2(CPM) of select subset of DEGs in *Chd4*$^{\Delta\beta}$ β-cells. *C*: Left, Venn diagram of differentially expressed (DE) *Chd4*$^{\Delta\beta}$ genes overlaid with Pdx1-bound genes obtained from ChIP experimentation of primary mouse islets (22), and right, biological processes of the 385 overlapping genes identified by GO analysis include those associated with nervous system development, signal transduction, regulation of ion transmembrane (transmem) transport, and hormone secretion. *n* = 4. FC, fold change; FDR, false discovery rate.

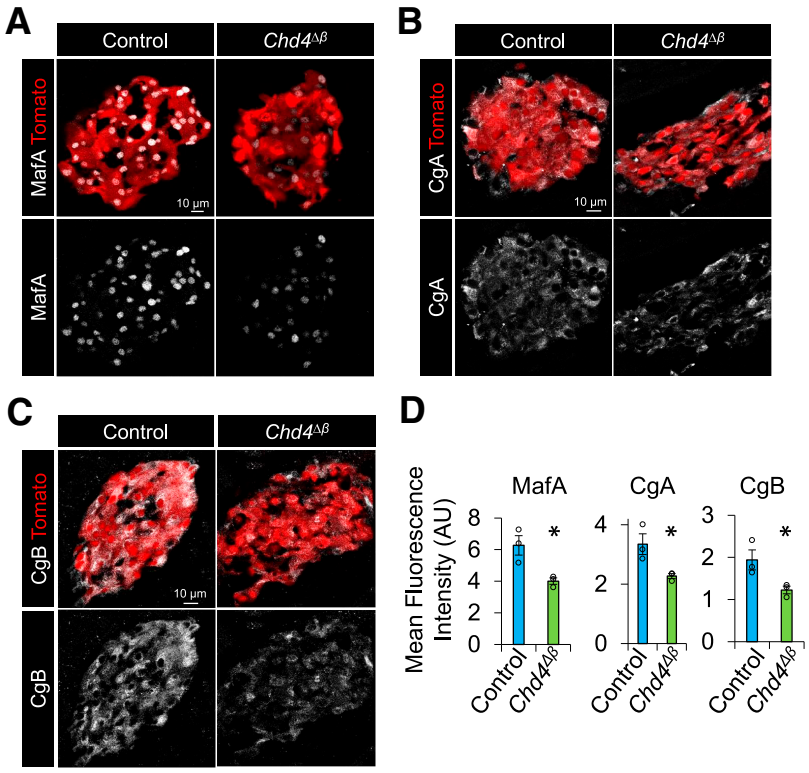


**Figure 4**—*Chd4*$^{\Delta\beta}$ β-cells have reduced levels of MafA, chromogranin A, and chromogranin B. Representative confocal images of islet-enriched TF MafA (*A*), chromogranin A (CgA) (*B*), and chromogranin B (CgB) (*C*) reveal that levels are compromised in lineage-labeled *Chd4*$^{\Delta\beta}$ β-cells. Scale bar = 10 μm. *D*: Mean fluorescence intensity of MafA, CgA, and CgB was calculated from Tomato$^{+}$ β-cells of control and *Chd4*$^{\Delta\beta}$ islets. AU, arbitrary units.

islets are treated under KCl-mediated depolarizing conditions (Fig. 2*A*).

### Immature-to-Mature Insulin Granule Ratios and Proinsulin Levels Are Elevated in *Chd4*$^{\Delta\beta}$ Mutants

The reductions in CgA and CgB could partially explain the defects in insulin secretion from *Chd4*$^{\Delta\beta}$ β-cells. Loss of CgB obstructs proinsulin processing leading to accumulation of proinsulin content in β-cells and causes an accumulation of immature insulin secretory granules (23,24). Therefore, we used transmission electron microscopy to provide detailed visualization of the cytoarchitecture of male control and *Chd4*$^{\Delta\beta}$ islets. We quantitated the number of mature, immature, and rod-like granules throughout and observed an increased percentage of immature insulin granules in male *Chd4*$^{\Delta\beta}$ islets (Fig. 5*A* and *B*). Accumulation of immature secretory granules could be resultant from defects in proinsulin conversion to insulin. In support of this idea, we found that male *Chd4*$^{\Delta\beta}$ islet contents have increased proinsulin-to-insulin ratios (Fig. 5*C*). Next, plasma collected from male *Chd4*$^{\Delta\beta}$ mutant mice 2 min following a glucose injection revealed that *Chd4*$^{\Delta\beta}$ mutants secreted significantly more proinsulin into the bloodstream and that overall proinsulin-to-insulin ratios were increased in *Chd4*$^{\Delta\beta}$ mutants (Fig. 5*D* and *E*).

### Chromatin Accessibility Is Significantly Altered in *Chd4*$^{\Delta\beta}$ β-Cells

To interrogate chromatin architecture changes in the *Chd4*$^{\Delta\beta}$ mutants, we performed ATAC-Seq on flow-sorted Tomato$^{+}$ cells from dispersed male control and *Chd4*$^{\Delta\beta}$ islets. Interestingly, of the DAC regions identified in *Chd4*$^{\Delta\beta}$ β-cells, 872 resided within promoters (±1 kb from transcription start site [TSS]) (Fig. 6*A*), corresponding to 81 genes with closed and 791 genes with open chromatin in *Chd4*$^{\Delta\beta}$ β-cells. Of the 791 genes with open chromatin at the promoter, 218 were upregulated, and 12 of the 81 genes with closed chromatin were downregulated, in *Chd4*$^{\Delta\beta}$ β-cells. In GO pathway analyses, these concordant overlapping genes were linked to pathways associated with regulation of insulin secretion and $K^{+}$ export across plasma membrane (Fig. 6*A* and Supplementary Table 4). We next aligned DAC regions from *Chd4*$^{\Delta\beta}$ β-cells with those defined to be functional enhancers within islets (25). There were 283 defined islet-enhancer regions that were differentially accessible in *Chd4*$^{\Delta\beta}$ β-cells. Of the genes associated with those enhancers, 12 were differentially expressed in *Chd4*$^{\Delta\beta}$ β-cells, including *MafA* (Supplementary Table 5).

Previously, we established that Chd4 binds to an upstream *MafA* regulatory sequence termed region 3 (base pairs −8118 to −7750 relative to the TSS [26]) in rodent β-cell lines (8). In support of this, across replicate samples, we observed *MafA* region 3 is in a more closed chromatin state (Fig. 6*B*).

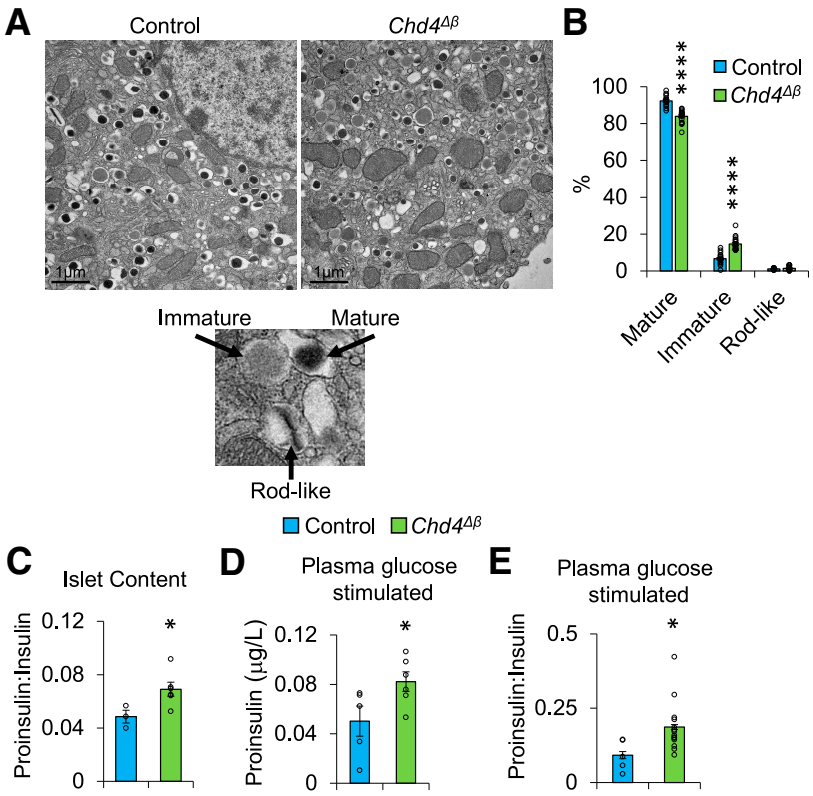


**Figure 5**—Loss of Chd4 results in increased immature granule number and increased proinsulin-to-insulin ratios. *A*: Representative electron microscopic images of β-cells and insulin granule morphology from control and *Chd4*$^{\Delta\beta}$ male islets. *B*: The percentages of immature, mature, and rod-like granules were calculated, revealing that *Chd4*$^{\Delta\beta}$ β-cells have elevated immature-to-mature granule ratios (scale bar = 1 μm) ($n$ = 4–5; 20 images per group quantitated). *C*: Ratio of proinsulin and insulin was determined from islets grown overnight in standard islet culture media (RPMI; 11 mmol/L glucose) ($n$ = 3–6). *D* and *E*: Plasma collected from fasted control and *Chd4*$^{\Delta\beta}$ male mice 2 min following stimulation with glucose revealed elevated plasma proinsulin levels and increased plasma proinsulin-to-insulin ratios ($n$ = 6–12). *$P < 0.05$; ****$P < 0.0001$.

Moreover, we found that *Slc2a2* (encoding the Glut2 primary glucose transporter in the rodent β-cell) expression is reduced (Fig. 3*A* and *B*), with chromatin accessibility being compromised at the promoter and intragenic regions (Supplementary Fig. 5). In a concordant manner, accessible chromatin signals were enhanced at promoter sites of genes upregulated in *Chd4*$^{\Delta\beta}$ β-cells, including *Kcnk5* and *Serpina1a* (Fig. 6*C* and Supplementary Fig. 5). Interestingly, we found differential regulation of alternate Chd members of the same class II Chd family. Whereas *Chd5* was found to be upregulated and promoter/intragenic regions showed increased chromatin accessibility in *Chd4*$^{\Delta\beta}$ β-cells (Supplementary Fig. 5), transcript levels of *Chd3* were unchanged in *Chd4*$^{\Delta\beta}$ β-cells. Interestingly, we observed that both Chd3 and Chd5 proteins are elevated in Tomato$^{+}$ *Chd4*$^{\Delta\beta}$ β-cells (Supplementary Fig. 4*B*). These data suggest partial compensation or possible functional redundancy by alternate Chd helicase subunits in the absence of Chd4, albeit to a degree that does not fully rescue the loss of Chd4.

We observed a relatively small number of differentially expressed genes (DEGs) in *Chd4*$^{\Delta\beta}$ β-cells that overlap with Pdx1-bound genes (Fig. 3*C*). Those DEGs not bound by Pdx1 suggest that the differences could be driven by either secondary effects, or, most likely, other islet-enriched TFs that are modulated by Chd4 activity. To this end, we performed HOMER analysis on our ATAC-Seq data set. As expected, a conserved homeobox-domain binding site (TAAT) was found to be a region with DAC at promoter regions (Supplementary Fig. 6*A*). There are several islet-enriched TFs, including Pdx1, that bind to this consensus sequence in the islet (Supplementary Fig. 6*A*). Additionally, binding sites for NeuroD1 and Smad proteins were identified at both promoter and enhancer regions (Supplementary Fig. 6*A* and *B*), opening the possibility that Chd4 is being recruited by these TFs to genomic control regions. NeuroD1 is of particular interest, as global deletion leads to arrest of islet development, loss of final β-cell mass, severe hyperglycemia, and perinatal death (27). To further interrogate the relationship between Chd4 and NeuroD1 in the β-cell, we analyzed ChIP-sequencing data sets for NeuroD1-occupied enhancer loci in mouse islets, which were also flanked by H3K4me1-marked nucleosomes (28), to evaluate their overlap with *Chd4*$^{\Delta\beta}$ DEGs and those bound by Pdx1 (from mouse islets [22]). We revealed a notable overlap of genes bound by both Pdx1 and NeuroD1, with 74 of *Chd4*$^{\Delta\beta}$ DEGs found in all three gene sets (Supplementary Fig. 7). Those genes in all three data sets include β-cell functional

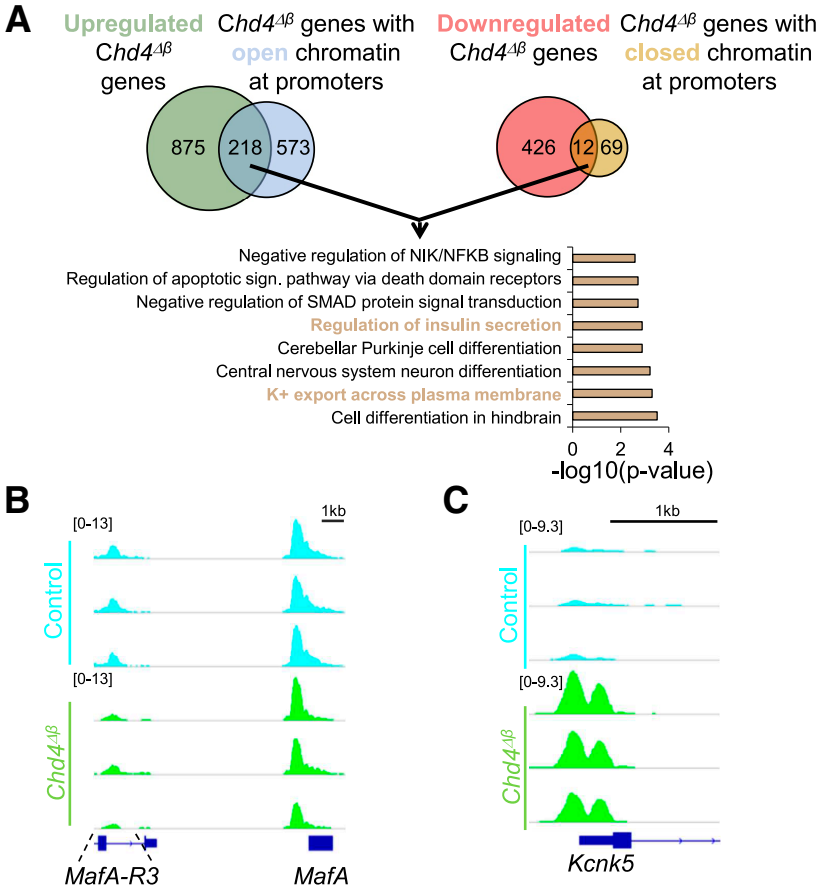


**Figure 6**—Chromatin accessibility is significantly altered at subset of gene promoters and defined islet enhancers in *Chd4*$^{\Delta\beta}$ β-cells. *A*: ATAC-Seq performed on FACS-sorted, Tomato$^{+}$ control and *Chd4*$^{\Delta\beta}$ male β-cells ($n$ = 3) revealed numerous areas of DAC. Of these DAC regions, 872 peaks resided within gene promoter regions (±1 kb of TSS). In a concordant manner, 218 of the 791 genes with open chromatin were upregulated, and 12 of the 81 genes with closed chromatin were downregulated, in *Chd4*$^{\Delta\beta}$ β-cells. Biological processes of the 230 genes identified by GO analysis revealed pathways associated with regulation of insulin secretion and $K^{+}$ export across plasma membrane. *B* and *C*: Representative ATAC-Seq tracks of the enhancer *MafA* region 3 (*MafA-R3*) illustrating reduced chromatin accessibility (*B*) and *Kcnk5* promoter illustrating increased chromatin accessibility (*C*). sign., signaling.

genes such as *Robo2*, *Slc2a2*, and *Chga* (Supplementary Table 6). There was a relatively small number of *Chd4*$^{\Delta\beta}$ DEGs that reside in NeuroD1-bound genes (23 genes), suggesting other islet-enriched TFs are also likely being governed by Chd4.

### CHD4 Is Necessary for Insulin Secretion in EndoC-βH1 Cells

We next assessed the functional role of human *CHD4* using siRNA in the well-characterized human β-cell line model, EndoC-βH1 cells. *CHD4* levels were reduced ∼50% from EndoC-βH1 cells following siRNA-mediated depletion (Fig. 7*A*). Analyses of various genes linked to β-cell function and those differentially expressed in *Chd4*$^{\Delta\beta}$ β-cells revealed significant reductions in *MAFA*, *G6PC2*, and *INS* (Fig. 7*B*). The reduced expression of *INS* was not expected, as levels of *Ins1* and *Ins2* are unchanged in both *Chd4*$^{\Delta\beta}$ β-cells and rodent β-cell lines following transient knockdown of *Chd4* (8). GSIS following *CHD4* knockdown in EndoC-βH1 cells revealed a marked reduction in insulin secretion, with no significant alteration in insulin content (Fig. 7*C* and *D*). In agreement with observations from *Chd4*$^{\Delta\beta}$ islets, we reveal a trending elevation of proinsulin and proinsulin-to-insulin ratios in EndoC-βH1 cell contents following knockdown of CHD4 (Fig. 7*E* and *F*).

## DISCUSSION

Blood glucose homeostasis requires adapted responses from hormone-secreting islet cells and hormone-sensitive peripheral tissues such as liver, muscle, and adipose cells. The adaptation by the islet β-cell is largely regulated at the transcriptional level, through interaction among DNA-bound TFs, recruited transcriptional coregulators, and the basal transcriptional machinery. Although numerous coregulators with diverse enzymatic activities exist in mammalian cells, few have been characterized to govern the activities of islet-enriched TFs. We previously showed that interactions between Pdx1 and the Chd4 subunit of the NuRD complex are amplified under acute glucose stimulatory conditions and are significantly reduced in pathophysiological conditions associated with diabetes (8),

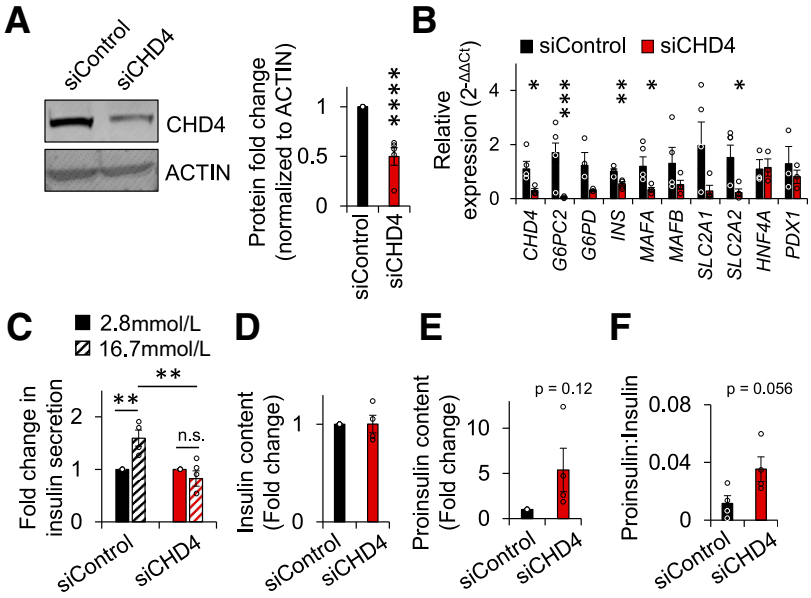


**Figure 7**—CHD4 modulates genes essential for insulin secretion in EndoC-βH1 human β-cell lines. *A*: Left, protein level of CHD4 was reduced on targeted siRNA treatment (siCHD4), and right, densitometric analysis indicated effective knockdown of *CHD4* ($n = 5$). *B*: The effect of *CHD4* knockdown on candidate β-cell mRNA levels was determined with quantitative PCR analyses ($n = 3$–4). *C* and *D*: GSIS was measured 1 h following glucose stimulation with 16.7 mmol/L glucose in cells treated with siRNA for 72 h. *C*: Results are presented as fold stimulation between siControl and siCHD4 at 16.7 vs. 2.8 mmol/L glucose following normalization to insulin content. Statistical analyses between groups were performed with one-way ANOVA with Tukey post hoc analysis. $^{**}P < 0.01$. n.s., not significant. Insulin (*D*) and proinsulin (*E*) content levels were monitored following knockdown ($n = 4$). *F*: Proinsulin-to-insulin ratios were calculated in unstimulated EndoC-βH1 cells following knockdown of *CHD4* ($n = 4$). $^{*}P < 0.05$; $^{**}P < 0.01$; $^{***}P < 0.001$; $^{****}P < 0.0001$.

suggesting that Chd4 is a modulator of Pdx1 activity and, therefore, β-cell function. Here, we report the importance of Chd4 in governing β-cell gene expression, chromatin accessibility, β-cell function, and mature insulin granule production in vivo.

In this regard, conditional removal of Chd4 from mature islet β-cells leads to disruptions of gene expression programs that induce glucose intolerance and impaired insulin secretion (Figs. 1 and 2). For example, we demonstrate that Chd4 has a prominent role in regulating *MafA*, a critical TF important for insulin secretion, by augmenting chromatin accessibility at Pdx1-regulated *MafA* region 3 enhancer (Figs. 3 and 6). Furthermore, we identified a role for Chd4 in positively regulating the genes encoding CgA and CgB, which are essential for appropriate granule maturation, and in maintaining appropriate proinsulin-to-insulin ratios in the β-cell (23,24,29). Interestingly, in addition to reduced mature granule density, we also found elevated proinsulin-to-insulin ratios in $Chd4^{\Delta\beta}$ islets (Fig. 5). Given the history of the $MIP\text{-}Cre^{ERT}$ and other transgenic Cre-driver lines in augmenting β-cell function (30), all control and experimental animals included $MIP\text{-}Cre^{ERT}$ and received tamoxifen. While we controlled for factors that could confound the results, this model is not without its limitations, as we are unable to distinguish any potential role of Chd4 in controlling Cre expression/activity or Tamoxifen actions within the β-cell.

Deletion of *Pdx1* from mature β-cells leads to loss of β-cell function and identity, where Pdx1-deficient cells acquire molecular and transcriptional signatures of α-cells, including expression of *Gcg* and *MafB* (31). This suggests that Pdx1 activates β-cell functional genes and represses non–β-cell genes. As Chd4 has been shown to maintain identity of a variety of cell types (e.g., cardiac muscle cells, skeletal muscle cells, embryonic stem cells), we expected to observe an increase in non–β-cell genes in Chd4-deficient β-cells. However, we did not observe upregulation of genes encoding non–β-cell hormones (e.g., *Gcg*, *Sst*, *Ppy*, *Ghrl*) (Supplementary Fig. 4), but we did detect changes in several disallowed genes (*Hk2*, *Pdgfra2*, *Mycl*, *Serpina* and *Serpine* family members) (Fig. 3), suggesting a partial reprogramming of the β-cell transcriptional state on Chd4 loss. Moreover, this indicates that other coregulators are contributing to the maintenance of Pdx1-repressive functions within the β-cell.

We found that β-cell–specific deletion of *Chd4* leads to increased chromatin accessibility and upregulation of an alternate Chd isoform, Chd5, and slightly elevated protein levels of Chd3 (Supplementary Fig. 4). This observation is consistent with our recent findings that transient knockdown of *Chd4* in mouse β-cell lines leads to upregulation of both *Chd3* and *Chd5* (8). Similarly, a satellite cell-specific deletion of *Chd4* led to upregulation of both *Chd3* and *Chd5*, which were additionally found to be bound directly by Chd4 (32). Interestingly, Chd5 has not garnered as much attention as Chd4, potentially due to having low expression in tissues outside the nervous system and testis (33). Whereas Chd5 might not

play major roles outside of these systems under physiological conditions, it could become important in situations where Chd4 activity is altered, such as the multisystemic neurodevelopmental disorder Sifrim-Hitz-Weiss, caused by missense mutations in *CHD4* (34). Therefore, the roles of other Chd subunits when Chd4 activity is altered will be an important avenue for future study.

Pdx1 interacts with a variety of transcriptional coregulators with various enzymatic functions in the β-cell (35). Loss of Chd4 leads to loss of expression of key β-cell functional genes, including *MafA* and *Slc2a2*, genes that are also regulated by the Swi/Snf chromatin remodeling complex (7). However, in contrast to Swi/Snf, whose activity is shown to promote Pdx1 occupancy to the *Ins2* locus and robust expression of *insulin* (7), Chd4 does not appear to alter expression of *Ins1* or *Ins2* or alter chromatin accessibility of their genomic loci (Supplementary Figs. 4 and 5). These findings underscore how the recruitment of different coregulators to distinct loci is imperative for proper gene regulation. Moreover, it raises the question as to how the selective recruitment of coregulators by Pdx1 to specific genomic loci is regulated. Whether potential posttranslational modifications of Pdx1 influence its ability to interact with specific coregulators remains to be established, as Pdx1 has been shown to undergo glycosylation, SUMOylation, ubiquitination, and phosphorylation (36–39), modifications that could alter its binding capacity and transcriptional activity.

We evaluated how transient loss of *CHD4* in human β-cell lines would impact gene expression signatures and islet function. Similar to $Chd4^{\Delta\beta}$ β-cells, we found reductions in *MAFA* and *SLC2A2* (Fig. 7). Interestingly, in EndoC-βH1 cell lines, reduced expression of *CHD4* also led to reduced expression of *INS*, which was unchanged in $Chd4^{\Delta\beta}$ mouse β-cells. Moreover, and in agreement with our mouse model findings, we revealed transient reduction in *CHD4* from EndoC-βH1 cells trends toward elevated proinsulin levels. However, in contrast to $Chd4^{\Delta\beta}$ islets, EndoC-βH1 insulin content was unchanged following knockdown. We propose that the differences likely arose from the transient siRNA knockdown in EndoC-βH1 cells with insufficient time having passed to reduce insulin content. However, while gene expression programs differ between mice and humans insufficient or deficient for *Chd4*, β-cell function was impaired in both models, demonstrating the importance for Chd4 in governing β-cell function across species.

Overall, our results demonstrate a prominent role of Chd4 in controlling insulin secretion and modulating a subset of gene targets within the β-cell to maintain its function. Our findings are the first to demonstrate that Chd4 plays an essential role in maintaining mature β-cell function in vivo. The regulation we characterized by Chd4 opens potential therapeutic opportunities to manage β-cell dysfunction associated with T2D.

**Acknowledgments.** The authors thank Lori Sussel (University of Colorado), Dylan Sarbaugh (University of Colorado), and Chad Hunter (University of Alabama at Birmingham) for critically reading the manuscript. The authors thank Katia Georgopoulos (Massachusetts General Hospital) for generously sharing the Chd4 floxed mice. The authors acknowledge the support of the Islet and Physiology and Translation Cores of the Indiana University School of Medicine Diabetes Research Center (National Institutes of Health grant P30-DK097512). Sequencing was carried out in the Center for Medical Genomics at Indiana University School of Medicine, which is partially supported by the Indiana University Grand Challenges Precision Health Initiative. The authors thank the members of the Indiana University Melvin and Bren Simon Comprehensive Cancer Center Flow Cytometry Resource Facility, which is partially supported by National Institutes of Health grants P30-CA082709 and U54-DK106846. The authors thank the Advanced Electron Microscopy Facility at University of Chicago for help in sample preparation and collection of transmission electron microscopy data.

**Funding.** This work was supported by grants from the National Institutes of Health National Institute of Diabetes and Digestive and Kidney Diseases (K01-DK115633, R03-DK127129, and R01-DK129287 to J.M.S.; F31-DK128918 to R.K.D.; R01-DK121929 and R01-DK133881 to E.K.S.; and R01-DK093954, R01-DK127236, and R01-DK127308 to C.E.-M.), the U.S. Department of Veterans Affairs Merit Award (I01-BX001733 to C.E.-M.), an award from the Ralph W. and Grace M. Showalter Research Trust and Indiana University School of Medicine (J.M.S.), bridge funding from the Herman B Wells Center for Pediatric Research (J.M.S.) and an Early Career Development Award from the Central Society for Clinical and Translational Research (J.M.S.).

**Duality of Interest.** No potential conflicts of interest relevant to this article were reported.

**Author Contributions.** R.K.D. and J.M.S. designed the study and drafted the manuscript. R.K.D., S.K., T.K., J.X., M.O., R.N.B., N.C., and J.M.S. executed the experiments. R.K.D., S.K., and J.M.S. performed data analysis. W.W. performed bioinformatics analysis. S.K., W.W., T.K., J.X., M.O., R.N.B., C.E.-M., and E.K.S. edited the manuscript. All authors read and approved the final manuscript. J.M.S. is the guarantor of this work and, as such, had full access to all the data in the study and takes responsibility for the integrity of the data and the accuracy of the data analysis.

**Prior Presentation.** Parts of this study were presented in abstract and oral presentation form at the 82nd Scientific Sessions of the American Diabetes Association, New Orleans, LA, 3–7 June 2022.

## References

1. Clapier CR, Cairns BR. The biology of chromatin remodeling complexes. Annu Rev Biochem 2009;78:273–304

2. Guo S, Dai C, Guo M, et al. Inactivation of specific β cell transcription factors in type 2 diabetes. J Clin Invest 2013;123:3305–3316

3. Shao S, Fang Z, Yu X, Zhang M. Transcription factors involved in glucose-stimulated insulin secretion of pancreatic beta cells. Biochem Biophys Res Commun 2009;384:401–404

4. Zhang F, Tanasa B, Merkurjev D, et al. Enhancer-bound LDB1 regulates a corticotrope promoter-pausing repression program. Proc Natl Acad Sci U S A 2015;112:1380–1385

5. Toren E, Liu Y, Bethea M, Wade A, Hunter CS. The Ldb1 transcriptional co-regulator is required for establishment and maintenance of the pancreatic endocrine lineage. FASEB J 2022;36:e22460

6. Scoville DW, Cyphert HA, Liao L, et al. MLL3 and MLL4 methyltransferases bind to the MAFA and MAFB transcription factors to regulate islet β-cell function. Diabetes 2015;64:3772–3783

7. Spaeth JM, Liu J-H, Peters D, et al. The Pdx1-bound Swi/Snf chromatin remodeling complex regulates pancreatic progenitor cell proliferation and mature islet β-cell function. Diabetes 2019;68:1806–1818

8. Davidson RK, Weaver SA, Casey N, et al. The Chd4 subunit of the NuRD complex regulates Pdx1-controlled genes involved in β-cell function. J Mol Endocrinol 2022;69:329–341

9. Tamarina NA, Roe MW, Philipson L. Characterization of mice expressing Ins1 gene promoter driven CreERT recombinase for conditional gene deletion in pancreatic β-cells. Islets 2014;6:e27685
10. Williams CJ, Naito T, Gómez-Del Arco P, et al. The chromatin remodeler Mi-2beta is required for CD4 expression and T cell development. Immunity 2004;20:719–733
11. Madisen L, Zwingman TA, Sunkin SM, et al. A robust and high-throughput Cre reporting and characterization system for the whole mouse brain. Nat Neurosci 2010;13:133–140
12. Stull ND, Breite A, McCarthy R, Tersey SA, Mirmira RG. Mouse islet of Langerhans isolation using a combination of purified collagenase and neutral protease. J Vis Exp 2012;67:4137
13. Buenrostro JD, Wu B, Chang HY, Greenleaf WJ. ATAC-seq: a method for assaying chromatin accessibility genome-wide. Curr Protoc Mol Biol 2015; 109:21.29.1–21.29.9
14. Heinz S, Benner C, Spann N, et al. Simple combinations of lineage-determining transcription factors prime cis-regulatory elements required for macrophage and B cell identities. Mol Cell 2010;38:576–589
15. Ravassard P, Hazhouz Y, Pechberty S, et al. A genetically engineered human pancreatic β cell line exhibiting glucose-inducible insulin secretion. J Clin Invest 2011;121:3589–3597
16. Livak KJ, Schmittgen TD. Analysis of relative gene expression data using real-time quantitative PCR and the 2(-delta delta C(T)) method. Methods 2001; 25:402–408
17. Brouwers B, de Faudeur G, Osipovich AB, et al. Impaired islet function in commonly used transgenic mouse lines due to human growth hormone minigene expression. Cell Metab 2014;20:979–990
18. Carboneau BA, Le TDV, Dunn JC, Gannon M. Unexpected effects of the MIP-CreER transgene and tamoxifen on β-cell growth in C57Bl6/J male mice. Physiol Rep 2016;4:e12863
19. Yang YHC, Manning Fox JE, Zhang KL, MacDonald PE, Johnson JD. Intraislet SLIT-ROBO signaling is required for beta-cell survival and potentiates insulin secretion. Proc Natl Acad Sci U S A 2013;110:16480–16485
20. Willmann SJ, Mueller NS, Engert S, et al. The global gene expression profile of the secondary transition during pancreatic development. Mech Dev 2016;139:51–64
21. Asplund O, Storm P, Chandra V, et al. Islet gene view-a tool to facilitate islet research. Life Sci Alliance 2022;5:e202201376
22. Khoo C, Yang J, Weinrott SA, et al. Research resource: the pdx1 cistrome of pancreatic islets. Mol Endocrinol 2012;26:521–533
23. Obermüller S, Calegari F, King A, et al. Defective secretion of islet hormones in chromogranin-B deficient mice. PLoS One 2010;5:e8936
24. Bearrows SC, Bauchle CJ, Becker M, Haldeman JM, Swaminathan S, Stephens SB. Chromogranin B regulates early-stage insulin granule trafficking from the Golgi in pancreatic islet β-cells. J Cell Sci 2019;132:jcs.231373
25. Gao T, Qian J. EnhancerAtlas 2.0: an updated resource with enhancer annotation in 586 tissue/cell types across nine species. Nucleic Acids Res 2019;2020;48:d58–D64
26. Raum JC, Gerrish K, Artner I, et al. FoxA2, Nkx2.2, and PDX-1 regulate islet beta-cell-specific mafA expression through conserved sequences located between base pairs -8118 and -7750 upstream from the transcription start site. Mol Cell Biol 2006;26:5735–5743
27. Naya FJ, Huang HP, Qiu Y, et al. Diabetes, defective pancreatic morphogenesis, and abnormal enteroendocrine differentiation in BETA2/NeuroD-deficient mice. Genes Dev 1997;11:2323–2334
28. Tennant BR, Robertson AG, Kramer M, et al. Identification and analysis of murine pancreatic islet enhancers. Diabetologia 2013;56:542–552
29. Wollam J, Mahata S, Riopel M, et al. Chromogranin A regulates vesicle storage and mitochondrial dynamics to influence insulin secretion. Cell Tissue Res 2017;368:487–501
30. Magnuson MA, Osipovich AB. Pancreas-specific Cre driver lines and considerations for their prudent use. Cell Metab 2013;18:9–20
31. Gao T, McKenna B, Li C, et al. Pdx1 maintains β cell identity and function by repressing an α cell program. Cell Metab 2014;19:259–271
32. Sreenivasan K, Rodríguez-delaRosa A, Kim J, et al. CHD4 ensures stem cell lineage fidelity during skeletal muscle regeneration. Stem Cell Reports 2021;16:2089–2098
33. Kolla V, Zhuang T, Higashi M, Naraparaju K, Brodeur GM. Role of CHD5 in human cancers: 10 years later. Cancer Res 2014;74:652–658
34. Weiss K, Lazar HP, Kurolap A, et al. The CHD4-related syndrome: a comprehensive investigation of the clinical spectrum, genotype-phenotype correlations, and molecular basis. Genet Med 2020;22:389–397
35. McKenna B, Guo M, Reynolds A, Hara M, Stein R. Dynamic recruitment of functionally distinct Swi/Snf chromatin remodeling complexes modulates Pdx1 activity in islet β cells. Cell Rep 2015;10:2032–2042
36. Gao Y, Miyazaki J-i, Hart GW. The transcription factor PDX-1 is post-translationally modified by O-linked N-acetylglucosamine and this modification is correlated with its DNA binding activity and insulin secretion in min6 beta-cells. Arch Biochem Biophys 2003;415:155–163
37. Kishi A, Nakamura T, Nishio Y, Maegawa H, Kashiwagi A. Sumoylation of Pdx1 is associated with its nuclear localization and insulin gene activation. Am J Physiol Endocrinol Metab 2003;284:E830–E840
38. Claiborn KC, Sachdeva MM, Cannon CE, Groff DN, Singer JD, Stoffers DA. Pcif1 modulates Pdx1 protein stability and pancreatic β cell function and survival in mice. J Clin Invest 2010;120:3713–3721
39. Frogne T, Sylvestersen KB, Kubicek S, Nielsen ML, Hecksher-Sørensen J. Pdx1 is post-translationally modified in vivo and serine 61 is the principal site of phosphorylation. PLoS One 2012;7:e35233